nano energy

RAPID COMMUNICATION

Self-powered velocity and trajectory tracking sensor array made of planar triboelectric nanogenerator pixels

CrossMark

Chang Bao Han[a], Chi Zhang[a], Xiao Hui Li[a], Limin Zhang[a],
Tao Zhou[a], Weiguo Hu[a], Zhong Lin Wang[a,b],*

[a]Beijing Institute of Nanoenergy and Nanosystems, Chinese Academy of Sciences, Beijing 100083, China
[b]School of Material Science and Engineering, Georgia Institute of Technology, Atlanta, GA 30332-0245, USA

Abstract
We report self-powered velocity and trajectory tracking sensor (VTTS) array for detecting object motion, velocity, acceleration and trajectory based on single-electrode triboelectric nanogenerator. The VTTS was fabricated by a cost-effective and simple-designed grid, which obtained the electric signals by the charge transition between the electrodes and the ground according to the electrostatic induction of objects. A self-powered VTTS arrays (9×9 pixels) with low-node mode was prepared and realized the real-time tracking of position, velocity, acceleration and trajectory for a moving object by visual observation. Using the simply electrode weave technique, a high-resolution VTTS with 41×41 pixels on an active size of $1 \times 1\ cm^2$ was obtained and it only needs the $41+41=82$ output ports. The device can detect a tiny displacement and trajectory for the high resolution of $250\ \mu m$. This work may provide a innovate design for preparing VTTS with ultrahigh pixels and low-cost.
© 2014 Elsevier Ltd. All rights reserved.

Introduction

A fast development of mobile electronics desperately needs the development of miniaturized power sources [1–3]. Even with a high-density energy storage unit, they will be drained out as a matter of time. Given this, the "self-powered" technology presents a possible approach for sustainable

*Corresponding author at: Beijing Institute of Nanoenergy and Nanosystems, Chinese Academy of Sciences, Beijing 100083, China.
  E-mail address: zlwang@gatech.edu (Z. Lin Wang).

operation of mobile electronics [4–6]. The device with self-powered system provides an independent, sustainable, maintenance-free operation and has a promising application in wireless sensor network [7,8], such as enzyme-based biosensors [9], condition monitoring system [10], or robot system [11]. Displacement tracking sensor is frequently used in today's smart phone and human tracking systems. However, a general design for this type of sensors is based on capacitive [12], optical [13,14], or magnetic [15], effects; a common characteristic of all these sensors is that they do need an external power source.

Recently, nanogenerators (NGs) [16–19] relying on the piezoelectric and triboelectric effects have been developed that convert mechanical energy in our living environment into electricity for powering gas sensor [20], liquid sensor [21], temperature sensor [22], skin sensor [23], speed sensor [24], and so on. The triboelecric nanogenerators (TENGs) offer not only a practical solution for self-powered devices [25,26], but also active sensors. For example, the detection of object motion inside of an one-dimensional (1-D) tube and in limited directions of a plane had been successfully realized based on single-electrode TENG [27,28]. A TENG array (7×7 cm^2) with the 8×7 pixels showed real-time tracking of the movement location [29].

In this work, a 2-D velocity and trajectory tracking sensor (VTTS) was fabricated by an ingenious electrode design based on an array of single-electrode TENGs [28,30]. The constructed active matrix of VTTS, combined with light-emitting diodes (LEDs), can achieve a self-powered, real-time position and trajectory tracking in 2-D plane. A device (1×1 cm^2) with pixels of 41×41 pixels was prepared and demonstrated exhibited high sensitivity. This work may provide a novel design for preparing self-powered VTTS with ultrahigh resolution.

Design and analysis

Theoretical analysis and working mechanism

When an object moves on a 2-D plane, it can be regarded as a plane rectangular coordinate system and whatever it locates in, as characterized by corresponding coordinates, (x, y). Conversely, provided that we had detected the coordinates of the object in real time, its velocity and trajectory was able to be obtained by X–Y data at the corresponding time. By further simplification, firstly the calculation of position and speed in 1-D direction were analyzed by the current signals at different x coordinates. Based on the single-electrode TENG, the working principle of the 1-D VTTS for location tracking is shown in Figure 1. The metal (Al) strips were fixed in parallel and each of the strips serves as an electrode of the single-electrode TENG and was connected to the output port. The width of PTFE (object), metal electrode and the spacing between the two electrodes are w, l and d, respectively. Each of the electrodes corresponds to the fixed location x_1, x_2, x_3, …. In the original position, the negative charges will be distributed on the surface of PTFE as a result of triboelectrification after a contact with Al. When the PTFE slides outward and approaches the electrode, the positive charges will flow from ground to the electrode and produced a negative current pulse (Figure 1(a)). Subsequently, it slides away from another edge of the electrode and a positive current peak will be generated. Therefore, the current signals indicate the location (x), from which we can know when and where the object moves to in 1-D direction, this is because that the object is electrostatically charged due to triboelectrification. Figure 1(b) displays the measured current change at different time when PTFE moves through different location (here, $w=l=10$ mm, $d=20$ mm).
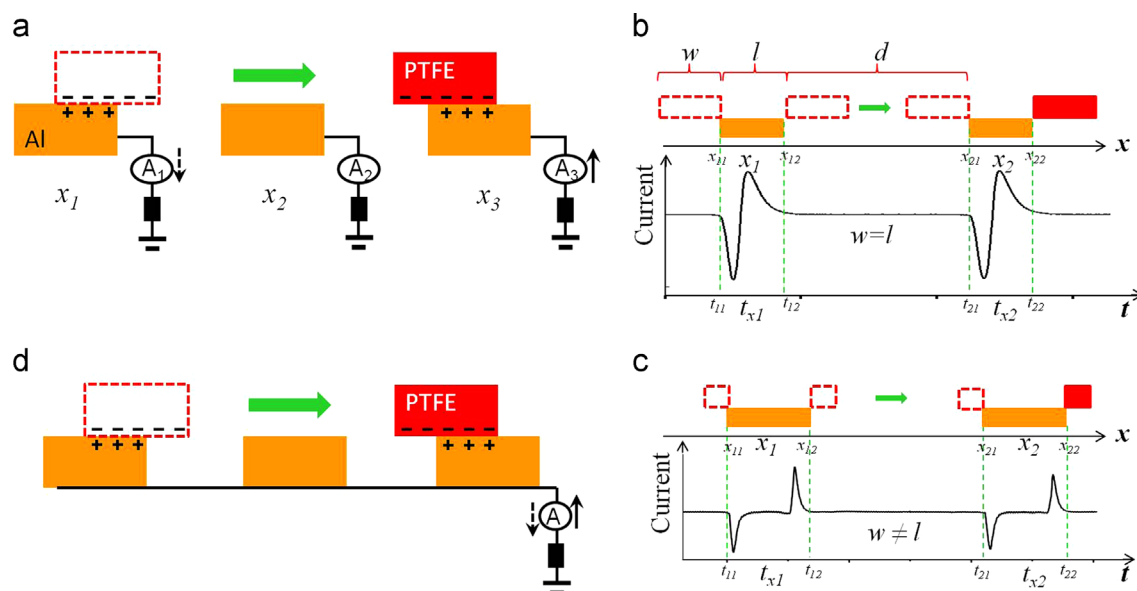

Figure 1 (a) and (d) are schematic diagrams of electricity-generation process in the 1-D direction for different types of electrode arrangements: individually grounded, and commonly grounded. (b) and (c) are the relationship among the movement, time and measured current signal of the sliders with different sizes in comparison to the width of the electrode, and the expected output signal shape.

For $w=l$, we assumed that the PTFE slides from x_1 to x_2 at the moment of t_1 and t_2. When the slider (PTFE) is just contacting and off the electrode, the corresponding locations and times are x_{11}, x_{12} and t_{11}, t_{12}. So the slider's speed v_1 when passing the location x_1 is

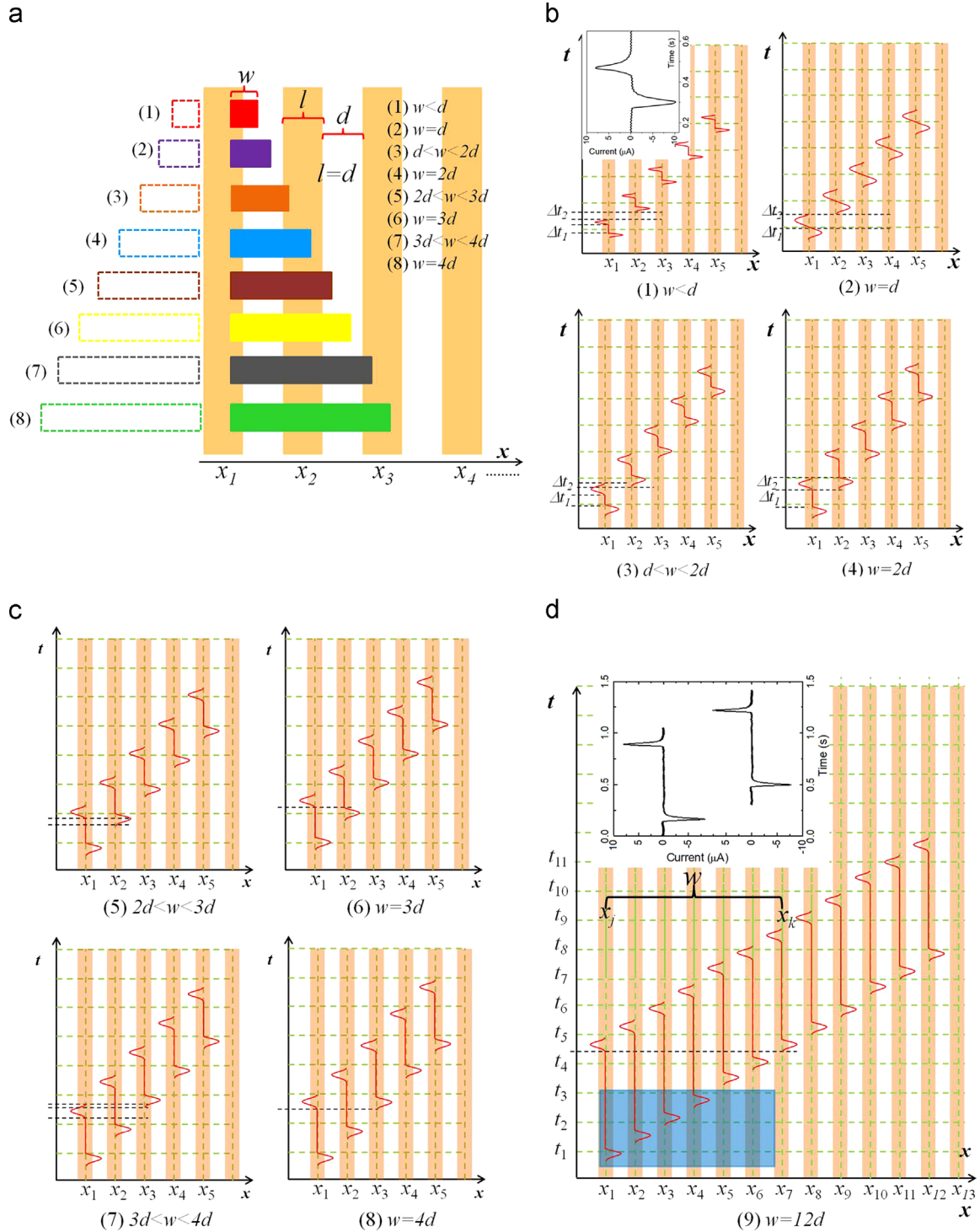$$v_1 = \frac{x_{12} - x_{11}}{t_{12} - t_{11}} = \frac{l}{\Delta t_{x1}} \tag{1}$$

Figure 2 (a) Schematic shows the sliders with different sizes moving across 1-D electrode arrays. (b), (c) and (d) are the location change versus time for different sizes of sliders according to the measured data. The inset of (b)(1) and (d) are one of the measured current-time relations corresponding to red curves.

similarly, the v_2 after sliding across x_2 is

$$v_2 = \frac{x_{22} - x_{21}}{t_{22} - t_{21}} = \frac{l}{\Delta t_{x2}} \qquad (2)$$

The average velocity $\overline{v}$ and acceleration a when the object moves from x_1 to x_2 are

$$\overline{v} = \frac{x_2 - x_1}{t_2 - t_1} = \frac{x_{21} - x_{11}}{t_{21} - t_{11}} = \frac{x_{22} - x_{12}}{t_{22} - t_{12}} = \frac{l + d}{\Delta t} \qquad (3)$$

$$a_{x_1 - x_2} = \frac{v_2 - v_1}{t_2 - t_1} \qquad (4)$$

If w is unequal to l, there will be an interval between the two inverse current peaks when PTFE passed by the electrode (Figure 1(c)). Here, the formulas of v_1, v_2, $\overline{v}$ and a are also applicable.

When the arrays of metal strips are connected linearly, it becomes a general single-electrode-based TENG and forms a joint output port (Figure 1(d)). If $w=l$, it will generate alternant current peaks as long as the PTFE sliding along the surface of electrodes one after another. Likewise, there has an interval between the two inverse current peaks when $w \neq l$. Therefore the current signals are similar to the curves shown in Figure 1(b) and (c). Both of the two structures (Figure 1(a) and (d)) are critical for designing and preparing the two-dimensional (2-D) VTTS.

1-D VTTS

The 1-D structure of VTTS with different situations is schematically illustrated in Figure 2(a). All of the electrode strips have the same size ($l=10$ mm) and are arranged uniformly with equal spacing. Every electrode corresponds to an output port and a location coordinate, x_1, x_2, x_3, and so on. Eight different widths of objects (PTFE) were analyzed when it slides across the electrode strips. The measured location changes at different time when the slider moves are shown in Figure 2(b). The red curves drawn by the measured data in the graph represent the current pulse or peak signal and also shows its direction, as well as the time of duration. The sliding was assumed to be uniform motion. For $w<l$ (for example, $w=8$ mm), a negative current peak appears when PTFE approaches the first electrode x_1. Then, the current pulse signal disappears when the slider is in the middle of the electrode and it generates a positive current pulse a moment later (Δt_1) from x_1 for sliding outward. This condition was depicted by red curves with reversed peak direction in Figure 2(b) (1) and it represent the same shape at the corresponding time. The inset of Figure 2(b)(1) is the measured current–time curve when the slider moves through a strip. After that, the current signal will disappear again for the time of Δt_2 and then the repetitive signals will be generated from the subsequent electrode. The speed during the PTFE sliding through the electrode x_1 is:

$$v_1 = \frac{l - w}{\Delta t_1} = \frac{d - w}{\Delta t_2} \qquad (5)$$

the width of slider is

$$w = \frac{l\Delta t_2 - d\Delta t_1}{\Delta t_2 - \Delta t_1} \qquad (6)$$

If $w=d$, the relationship between time and position can be more easily recognized (Figure 2(b)(2)). All of the current pulses are continuously in the time axis ($\Delta t_1 = \Delta t_2 = 0$). On the contrary, we concluded that the sliders have the same width with the electrode & spacing according to such graphs without calculation. If $d<w<2d$, the $\Delta t_1 > 0$ but $\Delta t_2 < 0$ (Figure 2(b) (3)). Eqs. (5) and (6) are also suitable for this condition. For other conditions, such as (4) $w=2d$, (5) $2d<w<3d$, (6) $w=3d$, (7) $3d<w<4d$, (8) $w=4d$, even $w=12d$ are depicted in Figure 2(b)(4), Figure 2(c) and (d), respectively. The above-mentioned formulas are suitable for all situations. If $w=2nd$ (n is an integer), the width of w could be clearly revealed by t-x relationships: $w=2(x_j - x_k)$ (Figure 2(d)).

However, usually the slider has a non-uniform motion. The average velocity and acceleration can still be calculated by Eqs. (1)-(4). The instantaneous velocity is approximated to be the average velocity during the sliding across one electrode. Hereby, the sensor with arrayed electrodes and corresponding output ports will record the object's speed (including average velocity, instantaneous velocity and acceleration) and location in 1-D direction.

2-D VTTS

Based on the design of 1-D VTTS, the 2-D structure of the sensor was constructed, as schematically illustrated in Figure 3. Firstly, the n numbers of metal strips were fixed equidistantly as x column and it corresponds to n numbers of output ports, x_1, x_2, ...x_n. Another m rows of electrodes then were vertically arranged as the output ports of y. Since the outputs from each cross-point should be independent, the intersection of electrodes x and y must be electrically insulated but other sections of electrodes should be in the same plane for intimately contact with the slider. Therefore, two types of structural design were introduced: low-node 2-D structure (Figure 3(a) and (b)) and crossed-node 2-D structure (Figure 3(c) and (d)). When the target object slides from A to D at an angle of θ, its movement can be resolved to the two vectors: x and y. Based on the analysis in Section 2.2, the final average velocity $\overline{v}$, instantaneous velocity v and acceleration a could be obtained by resultant vector:

$$\overline{v} = \sqrt{\overline{v}_x^2 - \overline{v}_y^2} \qquad (7)$$

$$v = \sqrt{v_x^2 - v_y^2} \qquad (8)$$

$$a = \sqrt{a_x^2 - a_y^2} \qquad (9)$$

moreover, the moving direction is

$$\theta = arctg\frac{v_y}{v_x} = arctg\frac{a_y}{a_x} \qquad (10)$$

if the object moves along x or y direction (A→C or A→D), the current signals from x and y output ports can be acquired based on the principle from Figure 1(a) and (c), respectively. Such 2-D grid design forms an active matrix sensor with high pixel resolution.
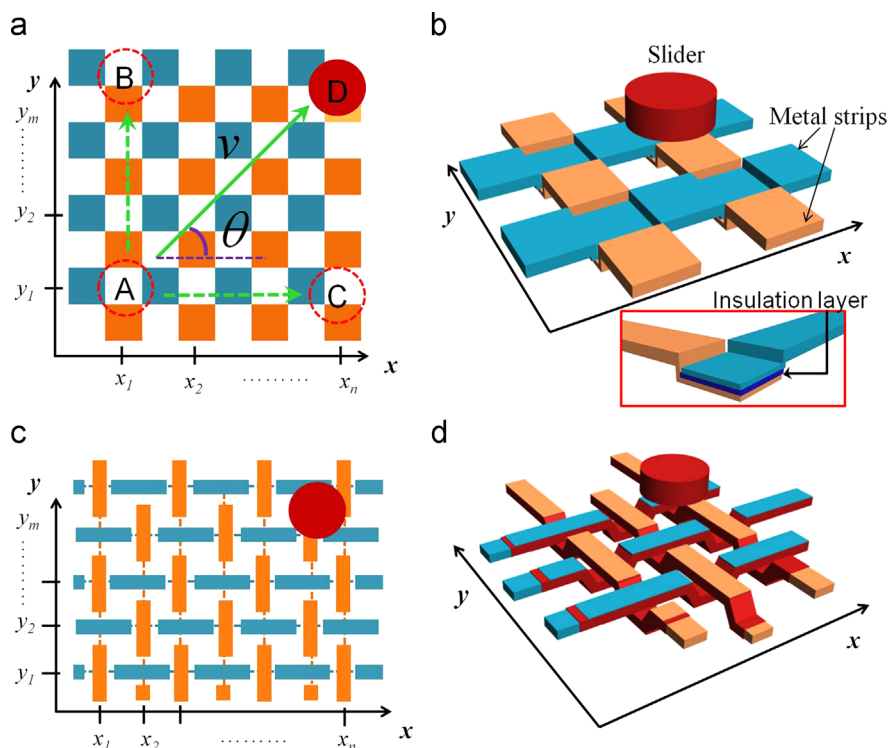
Figure 3 Schematic drawing of 2-D VTTS. (a) Top-view of 2-D structure sensor with low node; (b) the 3-D structure of sensor with low node; the inset is the 3-D structure of a node. There is an insulation layer between the top and bottom Al stripes so that they are not in direct contact. (c) Top-view of 2-D structure sensor with crossed node; and (d) the 3-D structure of sensor with crossed node.

Result and discussion

Self-powered and real-time VTTS

To demonstrate practical applications, a 9×9-pixel VTTS array low node was fabricated and schematically shown in Figure 4(a). Nine Al strips with a width of 6 mm were paralleled attached on acrylic glass (20 cm × 20 cm) as the different x output ports and an external load of 10 MΩ is connected between each electrode and the ground. The spacing (d) between the two electrodes is 14 mm. Similarly, another 9 rows of Al strips (20 cm × 0.6 cm) were vertically fixed on the substrate as y output ports. The nodes of electrode were below the surface and electrically insulated with each other (Supporting information, Figure "Appendix A"). Optical graph of the device is shown in Figure 4(b). A layer of PTFE film (13 mm × 13 mm) was treated by plasma surface treatment to form nanoscale structures for improving the surface areas and attached on the surface of target object (Figure 4(c)). When the object slides across one of electrodes, the open-circuit voltage, as shown in Figure 4(d), reaches the value of 70 V and the maximum short-current peak is beyond 6 μA (Figure 4(f)). So a row of LEDs are easily lighted up (Figure 4(e)), which affords a real-time vision image to tracking the movement of the object (Supporting information, video). In addition, the average velocity is calculated to be 2.8 cm/s using Eq. (5). When the object moves along a 2-D trajectory (Figure 4 (a)), such as sliding from A to B ("S" curve), the trajectory data are recorded by current signal from each output ports.

Figure 4(g) and (h) demonstrates the position change versus time, and any instantaneous velocity and acceleration could be calculated by the two curves. For example, the velocity, acceleration and angle at the position B are 22.5 cm/s, 0.2 cm/s^2, and 137°, respectively. Finally, moving trajectory in 2-D direction is displayed in the curves of x-y coordinates. Thus, a distinct "S" trajectory is shown in Figure 4(i). For achieving a direct observation, the fabricated VTTS can be used as a power source to light up commercial LEDs for real-time trajectory of movement and the intersection of the two rows of LEDs is the location. The photograph in Figure 4(j) clearly reveals the moving curve by tracking the intersection of lighted LEDs. Therefore, the VTTS, as a self-power sensor, can effectively track the movement.

Supplementary material related to this article can be found online at http://dx.doi.org/10.1016/j.nanoen.2014.07.025.

VTTS with fine pixels

To obtain the VTTS with high resolution but low cost, the 2-D structure with low node is difficult to be prepared except expensive micromachining. This problem can be solved by another design of VTTS with crossed node, which was mentioned in Section 2.3. The device was fabricated by simple weave technique using finer and insulated metal wires (Supporting information, Figure "Appendix A"). A basic design-knitting structure VTTS is sketched in Figure 5(a). Here, 41 x output ports and 41 y output ports
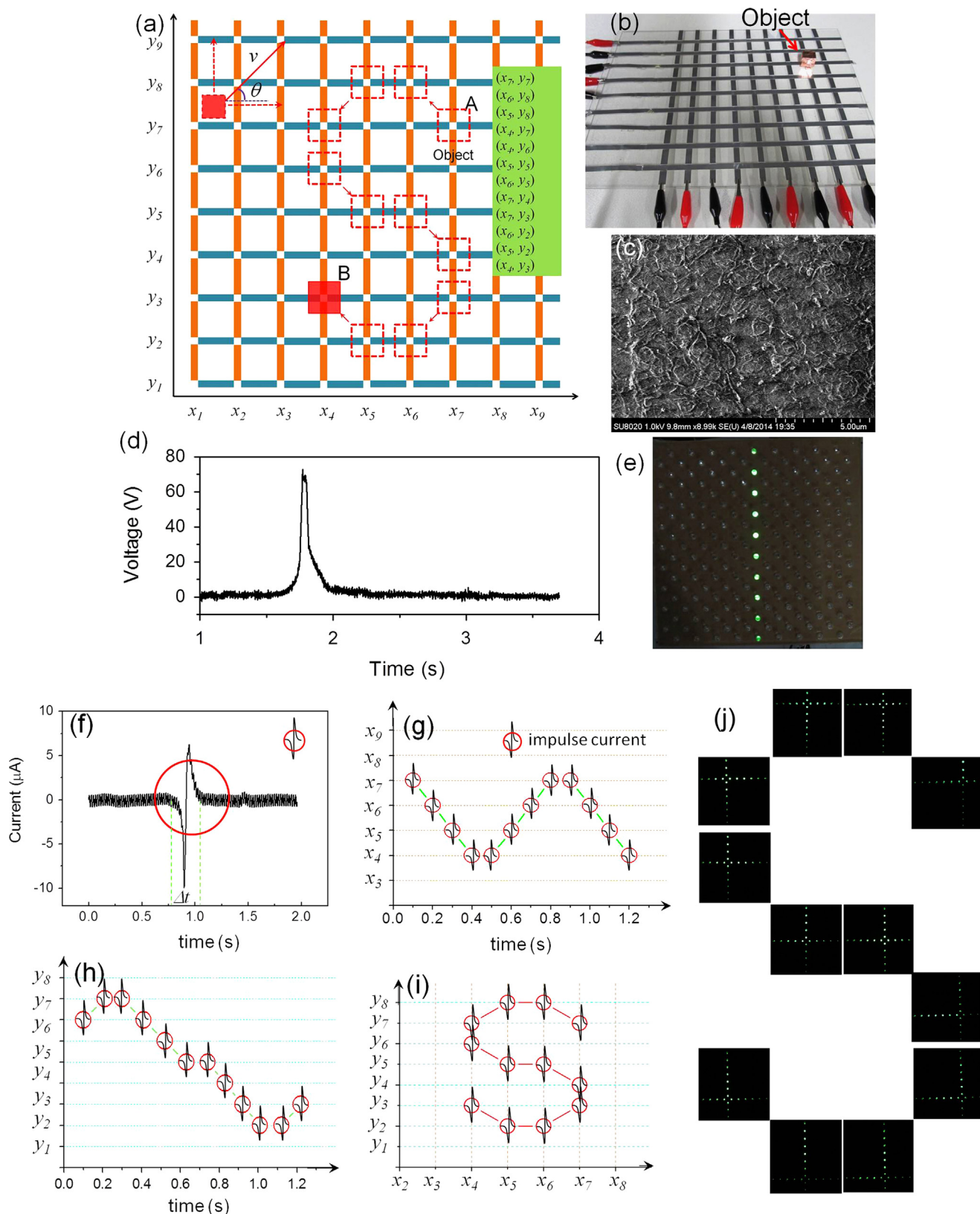
Figure 4 (a) Schematic diagram of 2-D VTTS with low node. The trajectory of the object is from A to B. (b) Optical image of the fabricated sensor. (c) SEM image of PTFE surface. (d) Open-circuit voltage of single output port. (e) Photograph of the LEDs array. (f) The current pulse signal from *x* output ports versus time. (g) The current pulse signal from *y* output ports versus time. (h) The current pulse signal from both *x* and *y*. (i) Output current of single output port. (j) A real-time location tracking photograph using LED bulbs as sensing indicators. The cross point of from *x* direction and *y* direction is the real-time position of object.
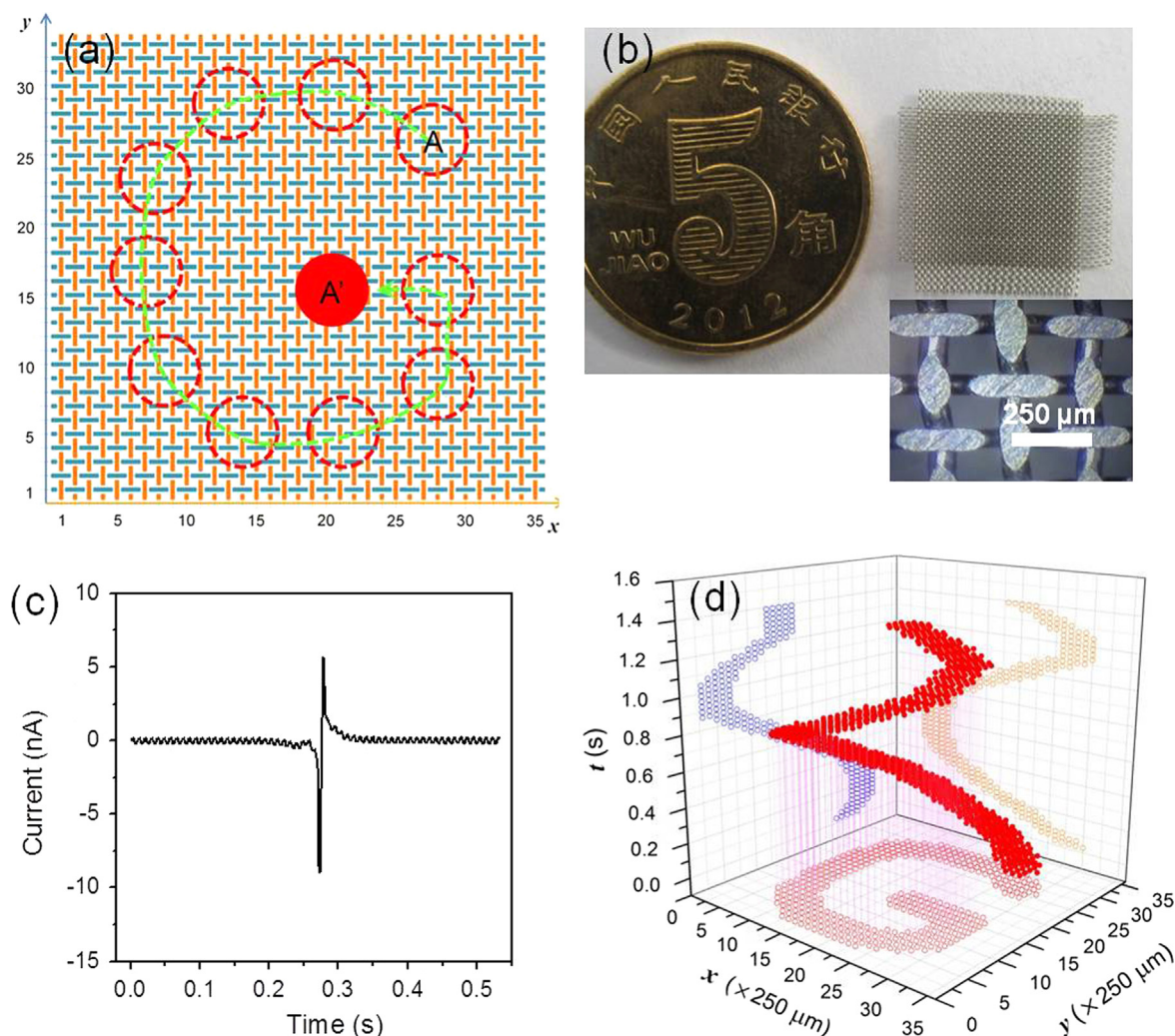
Figure 5 (a) Schematic diagrams of 2-D VTTS with crossed node and the trajectory of object. (b) Photo graph of VTTS with 41 × 41 pixels in size of 1 cm × 1 cm. (c) Output current of single output port. (d) The measured 3-D trajectory curves for the object.

were vertically interweaved forming a 41 × 41 = 1681 pixels on the grid structure (1 cm × 1 cm). The distance between the electrodes is 250 μm so the resolution of movement is 250 μm (inset of Figure 5(b)). An object (PTFE, with nanoscale on surface) with a diameter of ~1.3 mm (effective value) was introduced to slide along "G" curve on the surface of VTTS. The optical graph of the device is shown in Figure 5(b) and the inset is the high magnification graph. When the object slides across one of the electrode with the speed of 0.4 m/s, the peak of short-current reaches ~5 nA and the SNR (Signal to Noise Ratio) is about 50, which is sufficient enough for a sensor.

A 3-D experimental curve recording the motion trajectory of target object is shown in Figure 5(d), in which all of the data were tested only by 82 output ports. The x-t and y-t curves reveal the 2-D displacement component changing with time while the x-y curves afford the real-time trajectory of moving object. In the same way, the average velocity, instantaneous velocity and acceleration at any stage could be calculated. Besides, the approximate dimensions of the object is about 1.3 mm, which can also be

clearly found according to the width of trajectory line displaying in x-y coordinates form Figure 5(d) and it is consistent with the experimental data.

Conclusion

In summary, we demonstrate a simple and novel self-powered VTTS based on single-electrode triboelectrode nanogenerators. The generation of electric signals from every channel is based on the charge transfer between the metal strips or wires and the ground when an electrostatically charged object slides on the local surface of the device. Using the low-node designing, an active matrix VTTS with the 9 × 9 pixels was prepared to realize the real-time tracking of position, velocity, acceleration and trajectory by visual observation. Another high-resolution VTTS with 41 × 41 pixels and active size of 1 × 1 cm² was realized by simply electrode weave technique and obtained a clear position, velocity and trajectory data. This work may open up a brand-new approach to design and prepared VTTS with ultrahigh pixels and low-cost.

Experimental section

Surface modification of PTFE and Al

A layer of 30 μm PTFE thin film was cleaned with isopropyl alcohol and deionized water. Subsequently, plasma surface treatment equipment was used to prepare the nanoscale morphology on the surface of PTFE. In the etching process, the flow of O_2 and Ar are 10 and 12 sccm, respectively. A power source of 550 W was applied to generate a large density of plasma. For the VTTS with low node, the Al foil with the thickness of 100 μm was also cleaned with isopropyl alcohol and deionized water, and then was etched by sodium hydroxide solution (0.5 mol/L) in ultrasonic for 30 s for dissolving the oxide layer.

Fabrication of VTTS

For the VTTS with low node, a square-hole array (6.5×6.5 mm^2) was firstly processed on acrylic glass (the thickness of 4 mm) and the distance between holes was 2 cm. Then 9 columns and 9 rows Al strips were pasted on acrylic glass perpendicularly but also electrically insulated to each other. Here, there is an insulation layer between the top and bottom Al stripes so that they are not in direct contact. Every node is just in the square hole and below the level of strips. For VTTS with crossed node, the metal strips were replaced by finer metal wires with insulating varnish on its surface. Next, a 2-D metal grid was fabricated by simple weave technique. At last, the surface of grid was polished for wiping off the insulating varnish. The width of single electrode and the distance between electrodes are $\sim$80 μm and $\sim$250 μm, respectively. The matched load measured from the TENG based on single metal strip and PTFE was about 10 MΩ. So every output port was connected by an external load of 10 MΩ between each electrode and ground.

The fabrication of LED arrays is as follows. First, ten LEDs were tandem as a group forming a row or a column and connected to a strip. Then nine rows and nine columns of LEDs form 9×9 arrays. All the rows and columns have a common electrode connected to the ground.

Characterization and electrical measurement

The surface morphology of PTFE and Al film were characterized by scanning electron microscope (SEM, FEI-8020). The output performance of the sensor was measured by a combination of multichannel measurement system and Stanford Research System (SR 570 low-noise current amplifiers).

Acknowledgments

Appendix A.   Supporting information

Supplementary data associated with this article can be found in the online version at http://dx.doi.org/10.1016/j.nanoen.2014.07.025.

References

[1] B.L. Ellis, P. Knauth, T. Djenizian, Adv. Mater. 26 (2014) 3368-3397.
[2] M. Magno, D. Porcarelli, L. Benini, D. Brunelli, A Power-aware Multi Harvester Power Unit with Hydrogen Fuel Cell for Embedded Systems in Outdoor Applications, 2013 in: International Green Computing Conference (IGCC), 2013.
[3] J. Seunghun, S. Woong, C. Yeon-Gon, R. Soojung, Low-power Reconfigurable Audio Processor for Mobile Devices, 2014 in: Proceedings of IEEE International Conference on Consumer Electronics (ICCE), 2014.
[4] Z.L. Wang, Sci. Am. 298 (2008) 82-87.
[5] S. Xu, Y. Qin, C. Xu, Y.G. Wei, R.S. Yang, Z.L. Wang, Nat. Nanotechnol. 5 (2010) 366-373.
[6] Z.L. Wang, Adv. Mater. 24 (2012) 280-285.
[7] Z.L. Wang, Nano Today 5 (2010) 512-514.
[8] Y.F. Hu, Y. Zhang, C. Xu, L. Lin, R.L. Snyder, Z.L. Wang, Nano Lett. 11 (2011) 2572-2577.
[9] E. Katz, A.F. Bückmann, I. Willner, J. Am. Chem. Soc. 123 (2001) 10752-10753.
[10] E.P. James, M.J. Tudor, S.P. Beeby, N.R. Harris, P. Glynne-Jones, J.N. Ross, N.M. White, Sens. Actuators A: Phys. 110 (2004) 171-176.
[11] M. Goldfarb, E.J. Barth, M.A. Gogola, J.A. Wehrmeyer, Trans. Mechatron. IEEE/ASME 8 (2003) 254-262.
[12] M. Bazghaleh, S. Grainger, M. Mohammadzaheri, B. Cazzolato, T.-F. Lu, Sens. Actuators A: Phys. 198 (2013) 91-98.
[13] G.G. Yaralioglu, A. Atalar, S.R. Manalis, C.F. Quate, J. Appl. Phys. 83 (1998) 7405-7415.
[14] A.L. Arriaga, F. Bony, T. Bosch, Progress on Self-mixing Sensors for In-situ Displacement Measurement, 2013 IEEE 11th International Workshop of Electronics, Control, Measurement, Signals and their application to Mechatronics (ECMSM), 2013.
[15] M.M. Miller, G.A. Prinz, P. Lubitz, L. Hoines, J.J. Krebs, S.F. Cheng, F.G. Parsons, J. Appl. Phys. 81 (1997) 4284-4286.
[16] X.D. Wang, J.H. Song, J. Liu, Z.L. Wang, Science 316 (2007) 102-105.
[17] Y. Qin, X.D. Wang, Z.L. Wang, Nature 451 (2008) 809-813.
[18] F.R. Fan, Z.Q. Tian, Z.L. Wang, Nano Energy 1 (2012) 328-334.
[19] G. Zhu, J. Chen, T. Zhang, Q. Jing, Z.L. Wang, Nat. Commun. 5 (2014) 3426.
[20] X.Y. Xue, Y.X. Nie, B. He, L.L. Xing, Y. Zhang, Z.L. Wang, Nanotechnology 24 (2013) 225501.
[21] H.L. Zhang, Y. Yang, Y.J. Su, J. Chen, C.G. Hu, Z.K. Wu, Y. Liu, C.P. Wong, Y. Bando, Z.L. Wang, Nano Energy 2 (2013) 693-701.
[22] Y. Yang, Y.S. Zhou, J.M. Wu, Z.L. Wang, ACS Nano 6 (2012) 8456-8461.
[23] S. Lee, R. Hinchet, Y. Lee, Y. Yang, Z.H. Lin, G. Ardila, L. Montes, M. Mouis, Z.L. Wang, Adv. Funct. Mater. 24 (2014) 1163-1168.
[24] Y.F. Hu, C. Xu, Y. Zhang, L. Lin, R.L. Snyder, Z.L. Wang, Adv. Mater. 23 (2011) 4068-4071.
[25] Z.L. Wang, ACS Nano 7 (2013) 9533-9557.
[26] J. Chen, G. Zhu, W.Q. Yang, Q.S. Jing, P. Bai, Y. Yang, T.C. Hou, Z.L. Wang, Adv. Mater. 25 (2013) 6094-6099.
[27] Y. Su, G. Zhu, W. Yang, J. Yang, J. Chen, Q. Jing, Z. Wu, Y. Jiang, Z.L. Wang, ACS Nano 8 (2014) 3843-3850.

[28] Y. Yang, H.L. Zhang, J. Chen, Q.S. Jing, Y.S. Zhou, X.N. Wen, Z.L. Wang, ACS Nano 7 (2013) 7342–7351.
[29] Y. Yang, H. Zhang, X. Zhong, F. Yi, R. Yu, Y. Zhang, Z.L. Wang, ACS Appl. Mater. Interfaces 6 (2014) 3680–3688.
[30] Y. Yang, Y.S. Zhou, H.L. Zhang, Y. Liu, S.M. Lee, Z.L. Wang, Adv. Mater. 25 (2013) 6594–6601.

Dr. **Changbao Han** received his Ph.D degree from Zhengzhou University in 2012. He firstly fabricated the GaN/Si nano-heterostructure array LEDs and realized its near-infrared light emission with high monochromaticity by band-gap engineering. His research interests include the synthesis of semiconductor nano-materials, photoelectric device and applications of triboelectric nanogenerator.

Dr. **Chi Zhang** received his Ph.D degree from Tsinghua Univisity in 2009. After graduation, he worked in Tsinghua Univisity as a postdoc research fellow and NSK Ltd., Japan as a visiting scholar. His research interests are nanogenerator as active micro/nano-sensors, self-powered MEMS/NEMS, flexible electronics, and their applications in sensor networks and human machine interaction.
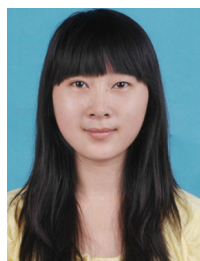
Xiaohui Li received her undergraduate degree from Zhengzhou University in 2013, and her major is Materials Science and Engineering, and now she is a First-year graduate student in Beijing Institute of Nanoenergy and Nanosystems, Chinese Academy of Sciences. Her research interests are focused on triboelectric nanogenerator, the luminescence of semiconductors, and their applications in sensor networks.

Limin Zhang received her undergraduate degree from Hebei University of Technology in 2012, and now she is a Second-year graduate student. Her research interests are piezoelectric nanogenerator and triboelectric nanogenerator, especially focus to nanogenerator as active micro/nano-sensors, flexible electronics and their applications in sensor networks and human machine interaction.

Tao Zhou received her master degree and bachelor degree from Harbin Institute of Technology in 2013 and 2011, respectively. Now she is a first-year doctoral candidate. Her research interests are piezoelectric nanogenerator and triboelectric nanogenerator, especially focus on nanogenerator as flexible and wearable power supplies, active sensors and their applications in wearable devices and wireless sensing systems.

Weiguo Hu is a professor of the institute of Beijing Institute of Nanoenergy and Nanosystems, Chinese Academy of Sciences (BINN, CAS). He got his Ph.D. degree at the Institute of Semiconductors, CAS 2007. In 2007–2011, he took his postdoctoral researches at Mie University and Kobe University. In 2011–2013, he he joined the Tohoku University as the assistant Professor. Since Sep. 2013, he joined the Beijing Institute of Nanoenergy and Nanosystems and took on novel piezotronic/piezophotonic devices.

Zhong Lin (ZL) received his Ph.D from Arizona State University in physics. He now is the Hightower Chair in Materials Science and Engineering, Regents' Professor, Engineering Distinguished Professor and Director, Center for Nanostructure Characterization, at Georgia Tech. Dr. Wang has made original and innovative contributions to the synthesis, discovery, characterization and understanding of fundamental physical properties of oxide nanobelts and nanowires, as well as applications of nanowires in energy sciences, electronics, optoelectronics and biological science. His discovery and breakthroughs in developing nanogenerators established the principle and technological road map for harvesting mechanical energy from environment and biological systems for powering a personal electronics. His research on self-powered nanosystems has inspired the worldwide effort in academia and industry for studying energy for micro-nano-systems, which is now a distinct disciplinary in energy research and future sensor networks. He coined and pioneered the field of piezotronics and piezo-phototronics by introducing piezoelectric potential gated charge transport process in fabricating new electronic and optoelectronic devices. Details can be found at: www.nanoscience.gatech.edu.